Toward the Elucidation of the Catalytic Mechanism of the Mono-ADP-Ribosyltransferase Activity of *Pseudomonas aeruginosa* Exotoxin A†

Souzan Armstrong and A. Rod Merrill*

Guelph-Waterloo Centre for Graduate Work in Chemistry and Biochemistry, Department of Chemistry and Biochemistry, University of Guelph, Ontario N1G 2W1 Canada

Received May 13, 2003; Revised Manuscript Received October 12, 2003

ABSTRACT: The catalytic mechanism for the mono-ADP-ribosyltransferase activity of *Pseudomonas aeruginosa* exotoxin A was investigated by steady-state and stopped-flow kinetic analyses. The rate constants for binding of the NAD^+ substrate to the enzyme were found to be $4.7 \pm 0.4\ \mu M^{-1}\ s^{-1}$ and $194 \pm 15\ s^{-1}$ for k_{on} and k_{off}, respectively. The k_{on} and k_{off} rate constants for the eEF-2 substrate binding to the enzyme were $320 \pm 39\ \mu M^{-1}\ s^{-1}$ and $131 \pm 22\ s^{-1}$, respectively. A potent, competitive inhibitor against the enzyme, 1,8-naphthalimide, bound the enzyme with k_{on} and k_{off} rates of $82 \pm 9\ \mu M^{-1}\ s^{-1}$ and $51 \pm 6\ s^{-1}$, respectively. Furthermore, the binding on and off rates for the reaction products, ADP-ribose and nicotinamide, were too rapid for detection with the stopped-flow technique. Investigation of the pre-steady-state kinetics for the ADP-ribose transferase activity of the toxin-enzyme showed that there is no pre-steady-state complex formed during the catalytic cycle. Binding of NAD^+ and smaller compounds representing the various parts of this substrate were investigated by the fluorescence quenching of the intrinsic toxin fluorescence. The binding data revealed a significant structural change in the enzyme upon NAD^+ binding that could not be accounted for on the basis of the sum of the structural changes induced by the various NAD^+ constituents. Product inhibition studies were conducted with nicotinamide and eEF-2-ADP-ribose, and the results indicate that the reaction involves a random-order ternary complex mechanism. Detailed kinetic analysis revealed that the eEF-2 substrate shows sigmoidal kinetic behavior with the enzyme, and fluorescence resonance energy transfer measurements indicated that wheat germ eEF-2 is oligomeric in solution.

Pseudomonas aeruginosa (PA)[1] is a ubiquitous, Gram-negative, opportunistic pathogen that is commonly found throughout the biosphere (*1*). It is one of the most important opportunistic bacterial pathogens in plants, animals, and humans (*2*). This ubiquitous organism has a high intrinsic resistance to antibiotics; hence, it is a leading cause of infections in AIDS, burn, cystic fibrosis, and post-operative patients and in other various immune-compromised human hosts (*3*). PA synthesizes a number of extracellular toxic products believed to be involved in the pathogenesis of these infections. The most toxic factor secreted by PA is the 66 kDa protein, exotoxin A (ETA). ETA belongs to a larger family of enzymes that catalyze the transfer of ADP-ribosyl moiety from NAD^+ to acceptors (*4*, *5*). More specifically, ETA is a member of the family of enzymes known as mono-(ADP-ribosyl) transferases (*6*−*8*) and is an NAD^+-diphthamide ADP-ribosyl transferase (EC 2.4.2.36). The enzyme domain of ETA catalyzes the transfer of ADP-ribose from NAD^+ to the diphthamide residue in eukaryotic translation factor protein, eEF-2. A catalytic mechanism based on the X-ray structure (*9*, *10*) and our own recent work has been proposed for this reaction (*11*−*13*). Previously, considerable work has been conducted on the catalytic mechanism of diphtheria toxin (DT), also a diphthamide-specific transferase, by Collier and co-workers (*14*−*17*), but rigorous kinetic analysis has not been conducted on the PA enzyme. Earlier, Schramm and co-workers modeled the active site of DT, and they proposed a transition state structure for the hydrolysis of NAD^+ based on kinetic isotope effects of isotopically labeled NAD^+s (*18*, *19*). Although this structure lacks the eEF-2 second substrate, it represents a convenient initial focal point in the understanding of the catalytic mechanism for both DT and ETA.

Although elucidation of the three-dimensional structure (*9*, *10*) and other approaches based on site-directed mutagenesis (*20*) and photoaffinity labeling (*21*, *22*) has provided valuable insights into the nature of amino acid residues

† Supported by the Canadian Institutes of Health Research (A.R.M.).

* Corresponding author. Tel: (519) 824-4120 ext. 3806. Fax: (519) 766-1499. E-mail: rmerrill@uoguelph.ca.

[1] Abbreviations: ADPRT, ADP-ribosyltransferase; 5-AF, 5-acetamide fluorescein; 5-IAF, 5-iodoacetamide fluorescein; β-TAD^+, β-methylene-thiazole-4-carboxamide adenine dinucleotide; 3-D, three-dimensional; DT, diphtheria toxin; ϵ-AMP, 1,N^6-etheno adenosine-5′monophosphate; ϵ-ADP, 1,N^6-etheno adenosine-5′diphosphate; eEF-2, eukaryotic elongation factor-2; eEF-2-ADPr, eEF-2 labeled with ADP-ribose; eEF-2-ϵADPR, eEF-2 labeled with etheno-ADP-ribose; eEF-2-AF, eEF-2 conjugated with 5-aminofluorescein; ϵ_M, molar extinction coefficient; ϵ-NAD^+, N^6-etheno-β-nicotinamide adenine dinucleotide; ETA, *Pseudomonas aeruginosa* exotoxin A; FRET, fluorescence resonance energy transfer; IAEDANS, 5-[[[acetyl]amino]-ethyl]amino]-naphthalene-1-sulfonic acid; IPTG, isopropyl-β-D-thio-galactopyranoside; MWCO, molecular weight cutoff; NAD^+, β-nicotinamide adenine dinucleotide (oxidized form); NAP, 1,8-naphthalimide; PA, *Pseudomonas aeruginosa*; PE24H, *Pseudomonas aeruginosa* exotoxin A 24 kDa C-terminal fragment containing a hexaHistag; SDS−PAGE, sodium dodecyl sulfate polyacrylamide gel electrophoresis; TRIS, tris(hydroxy-methyl) aminomethane; WT, wild-type.

10.1021/bi034772u CCC: $27.50
Published on Web 12/06/2003

participating in the catalytic mechanism, a detailed picture of the ADPRT reaction still remains obscure. Recently, we developed a fluorescence-based ADPRT assay specific for exotoxin A that has facilitated an in-depth characterization of the kinetic parameters for this toxin-enzyme (*23*). Furthermore, we have identified a catalytic loop within this enzyme that modulates the transferase activity, and we proposed that this is accomplished by stabilization of the transition state for the reaction (*24*). Additionally, we characterized the interaction of the toxin-enzyme with its protein substrate, eEF-2, by fluorescence resonance energy transfer (FRET) analysis, and we determined the binding constant (K_d) for the enzyme−substrate interaction (*5*−*13*). Importantly, we convincingly demonstrated that the enzyme will bind the eEF-2 protein substrate in the absence of the NAD^+ substrate, which immediately raised the possibility for a random-order ternary complex mechanism for this mono-ADPRT enzyme (*13*).

In the present work, we studied the kinetic details for the ADPRT reaction catalyzed by ETA through the use of stopped-flow fluorescence spectroscopy. We have successfully measured the k_{on} and k_{off} rates for both substrates, a potent competitive inhibitor of the NAD^+ substrate, 1,8-naphalimide (NAP), and we have also investigated the pre-steady-state kinetics for the reaction. Furthermore, we conducted product inhibition studies and characterized the aggregation state of the eEF-2 substrate to propose a more detailed enzyme mechanism for the ADPRT reaction catalyzed by this toxin-enzyme.

EXPERIMENTAL PROCEDURES

Overexpression and Purification of PE24H. The 24-kDa recombinant fragment of ETA with a C-terminal His-tag (PE24H) was overexpressed in *Escherichia coli* and purified as previously described (*13*).

Purification of eEF-2. Wheat germ eEF-2 was purified from a natural source as previously described (*23*).

Site-Directed Mutagenesis. Single Cys mutant proteins were prepared for the PE24H protein using oligonucleotide-based mutagenesis procedures as described earlier (*13*). The desired mutation was verified by dideoxy DNA sequencing with an ABI Prism Model 377 DNA sequencer using dye termination and cycle sequencing with samples run on a 4.5% acrylamide gel.

Fluorescence Labeling of PE24H. The PE24H protein was labeled with the fluorescent reagent, IAEDANS, as detailed earlier (*13*). The labeling efficiency was calculated from the adduct absorbance values using the appropriate molar extinction coefficients of the attached fluorophore and the protein as previously documented (*13*), and the efficiency was determined to be near unity.

Fluorescence Labeling of eEF-2. Purified wheat germ eEF-2 protein was labeled with 5-iodoacetamide fluorescein as described previously (*13*).

Labeling eEF-2 with ϵADP-Ribose. A 0.5-mL reaction mixture containing 1 mg of wheat germ eEF-2 was incubated with 0.1 μg of PE24H enzyme, 500 μM ϵNAD^+ in 20 mM Tris-HCl, 200 mM KCl, 1 mM EDTA, pH 7.6 (buffer A) for 30 min with mild agitation at 25 °C. The reaction was diluted 4-fold with 20 mM Tris-HCl, 50 mM KCl, 5% glycerol, 1 mM EDTA, pH 7.2 buffer (buffer B) and then was loaded to a 5-mL column containing Affi-Gel Blue resin (Biorad, Mississauga, ON) equilibrated in buffer B. The sample was reloaded and recycled to the column for a total of three times. The column was then washed with 50 mL of buffer B, and then eEF-2 was eluted from the column with buffer C, which was identical to buffer B except that it contained 1 M KCl. The eluted eEF-2-ϵADPr protein was concentrated to 0.5 mL in an Amicon Centriprep (10 000 MWCO) concentrator (Amicon Inc., Danvers, MA), the sample was then applied to a disposable size-exclusion 10 DG column (Biorad, Mississauga, ON), and the column was developed with 20 mM Tris-HCl, 50 mM KCl, 1 mM EDTA, 5% glycerol, pH 7.9 buffer (buffer D).

Labeling eEF-2 with ADP-Ribose. The reaction conditions were identical with those described previously except that 5 mg of wheat germ eEF-2 was labeled with 0.5 μg of PE24H enzyme in a 1-mL reaction volume, and NAD^+ rather than ϵNAD^+ was used.

Size-Exclusion HPLC Analysis. An HPLC column (1.25 cm diameter × 30 cm length) packed with Superose-6 HPLC gel filtration medium (Amersham Biosciences, Baie d'Urfé, PQ) was used to determine the hydrodynamic radius of wheat germ eEF-2 under enzyme reaction solution conditions. The solvent used to develop the column was 20 mM Tris-HCl, 100 mM KCl, pH 7.9 buffer. The column was calibrated with two sets of molecular weight protein gel filtration standards. One set of standards (low MW set, Amersham Biosciences, Baie d'Urfé, PQ) included ribonuclease A (R_S, 16.4 Å), chymotrypsinogen A (R_S, 20.9 Å), ovalbumin (R_S, 30.5 Å), and albumin (35.5 Å). The second set (high MW set, Sigma Co., St. Louis, MO) included albumin (R_S, 35.5 Å), alcohol dehydrogenase (R_S, 45.5 Å), apoferritin (R_S, 61 Å), and thyroglobulin (R_S, 85 Å). A plot of Stokes' radius against $[-\log(K_{av})]^{1/2}$ gave best fit lines for the standard curves with correlation values between 0.991 and 0.995. The sample (200 μL) was then injected onto the column, which was previously equilibrated with buffer. The solvent was delivered with a Biorad HRLC Model 2700 with a flow rate of 0.5 mL/min, and the protein was detected by a Biorad Model 1706 UV absorption monitor set at 280 nm. Elution volumes (V_e) were used to calculate the K_{av} values for each sample where $K_{av} = (V_e - V_o/V_t - V_o)$. V_e is the elution volume of the sample, V_o is the column void volume, and V_t is the total bed volume of the column. The data were analyzed as described previously (*25*, *26*).

Steady-State Fluorescence and Spectroscopic Measurements. All steady-state fluorescence measurements were obtained using a PTI Alphascan spectrophotometer interfaced with a computer using Felix Version 1.21 software (Photon Technology International, Lawrenceville, NJ) and equipped with a water-jacketed sample chamber set to 25 °C. The PE24H-AEDANS emission spectra ($\lambda_{ex} = 337$ nm) were recorded for proteins in 50 mM NaCl, 20 mM Tris-HCl (pH 7.9) solution. The eEF-2-AF emission spectra ($\lambda_{ex} = 492$ nm) were obtained for proteins in 100 mM KCl, 20 mM Tris-HCl (pH 7.9) buffer.

Absorbance spectra were obtained at room temperature with a Varian Cary-300 double-beam absorption spectrometer (Varian Inc., Mississauga, ON). PE24H-AEDANS absorbance spectra were scanned from 260 to 400 nm in 50 mM NaCl, 20 mM Tris-HCl (pH 7.9) solution. eEF-2-AF (eEF-2 conjugated with 5-aminofluorescein), eEF-2-ϵADPr (eEF-2

labeled with etheno-ADP-ribose), and eEF-2-ADPr (eEF-2 labeled with ADP-ribose) absorbance spectra were recorded from 250 to 600 nm in buffer D.

Rapid Kinetic Data Collection. All rapid kinetic data were obtained at 25 °C with an Applied Photophysics model SX.17MV stopped-flow fluorescence spectrometer equipped with an excitation monochromator and using filter-based fluorescence emission detection (Applied Photophysics, Leatherhead, UK). Excitation slit widths were 4 nm, and a variety of interference and emission cutoff filters were used depending upon the nature of the fluorescence reporter in the sample. The kinetic traces shown are an average of six to eight individual traces or shots. Intrinsic protein fluorescence was monitored by 280 nm excitation, and emission was detected at right angles with a 320 nm emission cutoff filter. The pre-steady-state kinetics of the base-catalyzed hydrolysis of ϵNAD$^+$ and toxin-catalyzed ADPRT reaction was measured with excitation at 305 nm (4 nm band-pass), and emission was measured through a monochromator set at 405 nm (8 nm band-pass). The k_{on} and k_{off} rates for eEF-2-AF binding to PE24-AEDANS were measured by excitation at 337 nm and emission with a 580 nm interference filter (20 nm band-pass). All experiments were conducted under pseudo-first-order conditions. Rate constants and amplitudes were obtained by fitting the data to equations describing a single- or double-exponential growth/decay using the Applied Photophysics software, Version 4.25.

Fluorescence-Based ADPRT Assay. The NAD$^+$-dependent ADPRT activity for the various cysteine PE24H proteins and their corresponding protein adducts was determined as described by Armstrong and Merrill (*23*). Product inhibition studies were conducted with either nicotinamide or eEF-2-ADPr as inhibitor while varying each of the substrates, NAD$^+$ and eEF-2, in separate experiments to determine the nature (type) of inhibition exhibited by the respective products in the reaction mixture.

Quenching of Intrinsic Protein Fluorescence. The NAD$^+$-dependent quenching of the intrinsic tryptophan fluorescence in PE24H was used to determine the binding constants (K_d) for NAD$^+$, NAP inhibitor, nicotinamide, AMP, ADP, or ADP-ribose as described elsewhere (*11*, *12*).

Fluorescence-Based eEF-2 Binding Assay. The FRET-based assay was conducted as previously described (*13*). The dissociation constant for eEF-2 binding with PE24H was determined using the following equation as part of the nonlinear fitting routine within Origin 6.1 software (OriginLab, Northampton, MA): $\Delta F_i/\Delta F_{max} = ([\text{eEF-2}]B_{max})/(K_D + [\text{eEF-2}])$, where ΔF_i is the change in fluorescence intensity for each ligand (eEF-2) concentration upon macromolecular association, ΔF_{max} is the maximum change in fluorescence intensity at saturation of the ligand-binding site within PE24H, K_d is the dissociation constant for the binding of eEF-2 with PE24H, and B_{max} is the total PE24H concentration (number of binding sites if there is only one site per protein).

S585C-AEDANS was chosen as the control protein (*13*) to determine the K_d for eEF-2-AF binding and for the determination of the rate constants for binding and release. S585C and its adduct behave similarly to the wild-type enzyme in terms of its catalytic activity and NAD$^+$-binding and also this protein labeled with IAEDANS at near unity efficiency.

Table 1: Steady-State Kinetic Parameters for NAD$^+$ and eEF-2 Substrates

parameter	NAD$^+$	eEF-2
k_{cat} (s^{-1})	11 ± 1.4^a	12 ± 1.1^b
K_M (μM)	275 ± 52^a	20.0 ± 1.3^b
K_{cat}/K_M ($\mu M^{-1} s^{-1}$)^c	0.041 ± 0.005	0.60 ± 0.04

[a] Steady-state kinetic data were taken from Armstrong and Merrill (*23*). [b] Steady-state kinetic data calculated from the data shown in Figure 7A using $v_o = V_{max}[S]^n/(K_M + [S]^n)$ according to the Hill equation where $n = 2.0$. [c] Data were calculated from data shown above.

FRET Studies of eEF-2 Oligomers. A preparation of eEF-2 was divided into two parts; one was labeled with 5-IAF, and the other part was labeled with IAEDANS as previously described (*13*−*27*). A solution of eEF-2-AEDANS in 20 mM Tris-HCl, 50 mM KCl, pH 7.9 was titrated with eEF-2-AF by the sequential additions of a stock solution of the latter. Upon each addition of the donor to the sample, the entire fluorescence spectrum was collected with excitation at 337 nm, and the emission was scanned from 350 to 650 nm (2 nm band-passes for both excitation and emission). The data were corrected for the dilution factor and then were plotted as Q_F/Q_0 against eEF-2-AF acceptor mole fraction. The data curves were then fitted according to the model described by Veatch and Stryer (*28*) where the degree of association of eEF-2 monomers upon titration was assessed by measuring FRET from a donor population (eEF-2-AEDANS) to an acceptor population (eEF-2-AF). The derivation of the model for the association of channel peptides (eq 1) has been presented previously (*29*).

$$\frac{Q_F}{Q_0} = 1 + E - E(1 - a)^{n-1} \quad (1)$$

Q_F/Q_0, the relative quantum yield of the donor species, is a ratio of the quantum yield of the donor species in the presence (Q_F) and absence (Q_0) of the acceptor species. E represents the efficiency of the FRET process, a is the mole fraction of the acceptor species, and n is the number of eEF-2 monomers that comprise the oligomeric complex.

RESULTS

Steady-State Kinetic Parameters. The steady-state kinetic parameters for both substrates of the PE24H enzyme are summarized in Table 1. The toxin-enzyme shows conventional Michaelis−Menten kinetic behavior against the NAD$^+$ substrate with a K_m and specificity constant (k_{cat}/K_m) of 275 μM and 0.041 μM^{-1} s^{-1}, respectively. However, the enzyme exhibits sigmoidal kinetics against the protein substrate, eEF-2, with a lower K_m and hence a higher specificity constant (20.0 μM and 0.60 μM^{-1} s^{-1}, respectively) than for the dinucleotide substrate. The sigmoidal behavior for the eEF-2 substrate is believed to originate from the oligomeric state of this protein in solution, but other explanations are possible (see Results and Figure 7).

NAD$^+$ Binding and Rate Constants. Figure 1A shows the saturable binding curve for the titration of the PE24H enzyme with the NAD$^+$ substrate in the absence of the eEF-2 protein substrate. The binding was quantified from the signal obtained for the quenching of the intrinsic fluorescence of

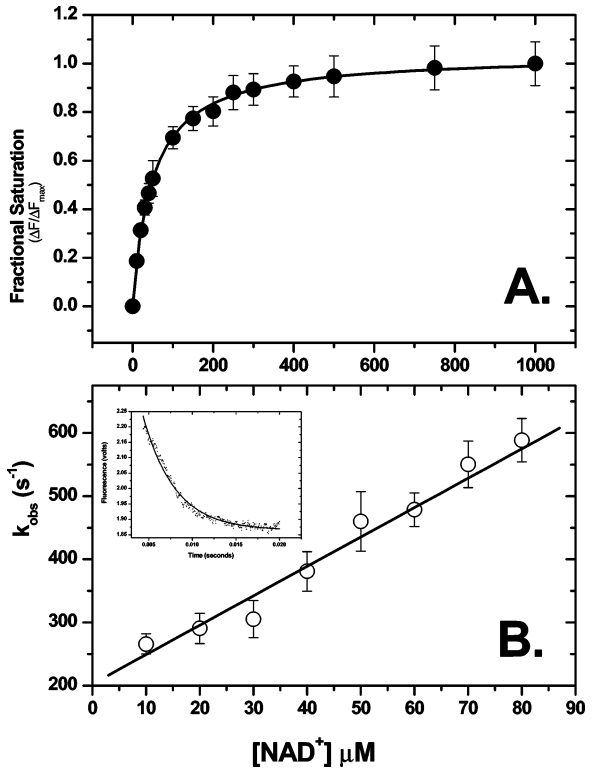

FIGURE 1: NAD^+ binding to PE24H. (A) The binding isotherm for NAD^+ with toxin as determined from the quenching of the intrinsic protein fluorescence. The raw fluorescence quenching data were converted to fractional saturation values ($\Delta F/\Delta F_{max}$, see Experimental Procedures) and are plotted against the NAD^+ concentration. The excitation was 295 nm, and the emission was 340 nm with excitation and emission band-passes at 4 nm in 20 mM Tris-HCl, 50 mM NaCl, pH 7.9 at 25 °C. The final concentration of PE24H was 1.25 μM, and NAD^+ was varied between 0 and 1000 μM. (B) The dependence of k_{obs} on the concentration of NAD^+ (10−80 μM). The inset shows the time-dependent fluorescence change associated with the binding of 50 μM NAD^+ to 1.0 μM PE24H.

Table 2: Kinetic and Thermodynamic Parameters for ADPRT Substrates and NAP Inhibitor of ETA

parameter	NAD^+	eEF-2	NAP[a]
k_{on}[b] (μM^{-1} s^{-1})	4.7 ± 0.4	320 ± 39	82 ± 9
k_{off}[b] (s^{-1})	194 ± 15	131 ± 22	51 ± 6
k_{off}/k_{on}[c] (μM)	41 ± 3	0.41 ± 0.10	0.62 ± 0.07
K_d[d] (μM)	45 ± 5	0.71 ± 0.21	0.054 ± 0.006 1.2 ± 0.1

[a] The inhibitor of the ADPRT reaction, 1,8-naphthalimide (*5*). [b] Determined by stopped-flow rapid binding measurements. [c] The dissociation constant as calculated from the ratio of the forward and reverse binding rate constants that were determined by stopped-flow measurements. [d] Determined from the equilibrium binding data shown in Figures 1A, 3A, 4A, and 5A.

the enzyme by the dinucleotide, NAD^+, as previously characterized (*11*, *12*). The dissociation constant (45 ± 5 μM) value is shown in Table 2 for this equilibrium binding experiment. The quenching of the Trp fluorescence observed at saturating NAD^+ concentration is significant and results in 16−20% of the original fluorescence signal (ref *12*; data not shown). The apparent (observed) binding rate constant for NAD^+ with PE24H was measured by stopped-flow fluorescence spectroscopy, and the data are plotted in Figure 1B. The plot of fluorescence emission intensity at 50 μM NAD^+ concentration as a function of time is shown in the inset to Figure 1B. The latter dataset for the time-dependent fluorescence change upon NAD^+ binding could be fit to a single-exponential function with a rate constant of 460 s^{-1}, and in fact, all of the datasets could be fit with a single-exponential function up to 90 μM. Unfortunately, the k_{obs} rate constants were too high to be accurately determined by the stopped-flow technique at NAD^+ concentrations above 90 μM. The association and dissociation rate constants, k_{on} and k_{off}, were determined from plots of k_{obs} versus [NAD^+] according to $k_{obs} = k_{on}[L] + k_{off}$. The values for the association and dissociation rate constants for the NAD^+ substrate with the enzyme are summarized in Table 2. Importantly, the dissociation constant (K_d) determined from equilibrium binding experiments was in good agreement with the value (k_{off}/k_{on}) calculated from the kinetic experiment (Table 2, 45 and 41 μM, respectively), adding credence to the kinetically derived k_{on} and k_{off} rates. Under pseudo-first-order conditions similar to those used for the determination of k_{cat} for the ADPRT reaction (Table 1; 500 μM ϵNAD^+ at 25 °C), the association rate for NAD^+ with the enzyme is 4.7 μM^{-1} s^{-1} × 500 μM = 2350 s^{-1}, which is approximately 200-fold greater than the k_{cat} value for the ADPRT activity of the toxin (Table 1).

Pre-Steady-State Kinetics. It is known that in solution NAD^+ exists as a folded structure (sandwich) with the two aromatic bases of the compound stacked against each other (*30*) and that when an enzyme binds this cofactor, separation of the adenine and nicotinamide ring systems ensues. Furthermore, when dehydrogenases bind to the fluorescent NAD^+ analogue, etheno-NAD^+ (ϵ-NAD^+), and it assumes the open conformation, it then has a much higher fluorescence quantum yield (*31*, *32*). The PE24H enzyme binds NAD^+ in a twisted horseshoe configuration (*33*), and it is expected that the fluorescence quantum yield of ϵ-NAD^+ would increase due to this interaction. Figure 2A shows that upon addition of enzyme (5 nM) to various solutions of ϵ-NAD^+ (50−800 μM) the rate of ϵ-NAD^+ fluorescence change increased in a linear fashion and was likely due to the breaking of the glycosidic bond between the C1 of ribose and the pyridinium N1 of nicotinamide and/or the transfer of ϵADP-ribose to eEF-2. To ascertain the source of the ϵ-NAD^+ fluorescence increase during steady-state kinetic experiments, the PE24H enzyme was added to a solution of ϵ-NAD^+ (Figure 2B) during fluorescence data acquisition. The binding of ϵ-NAD^+ to the toxin-enzyme did not cause any change in the fluorescence intensity of the ϵ-NAD^+ substrate (once the dilution factor was taken into account) unless this change occurred during the mixing time of the experiment (5 s) and featured a signal increase followed by a concomitant decrease in the fluorescence signal. At the end of the experiment, 50 mM NaOH was added (since it causes a large increase in the base-catalyzed hydrolysis of NAD^+) to verify that the ϵ-NAD^+ substrate was still largely intact (Figure 2B). To investigate the pre-steady-state kinetics on a more rapid time scale, the kinetic assay was conducted with a stopped-flow fluorescence spectrometer (Figure 2C,D). There was no evidence for the formation of a pre-steady intermediate upon base (OH^--catalyzed) hydrolysis of ϵ-NAD^+ (Figure 2C) on a time scale from 0.1 to 50 s, and furthermore, no intermediate was detected from 1.5 to 100 ms (Figure 2C, inset). Likewise, for the enzyme-catalyzed transfer of ϵADP-ribose from ϵ-NAD^+ to the diphthamide residue on

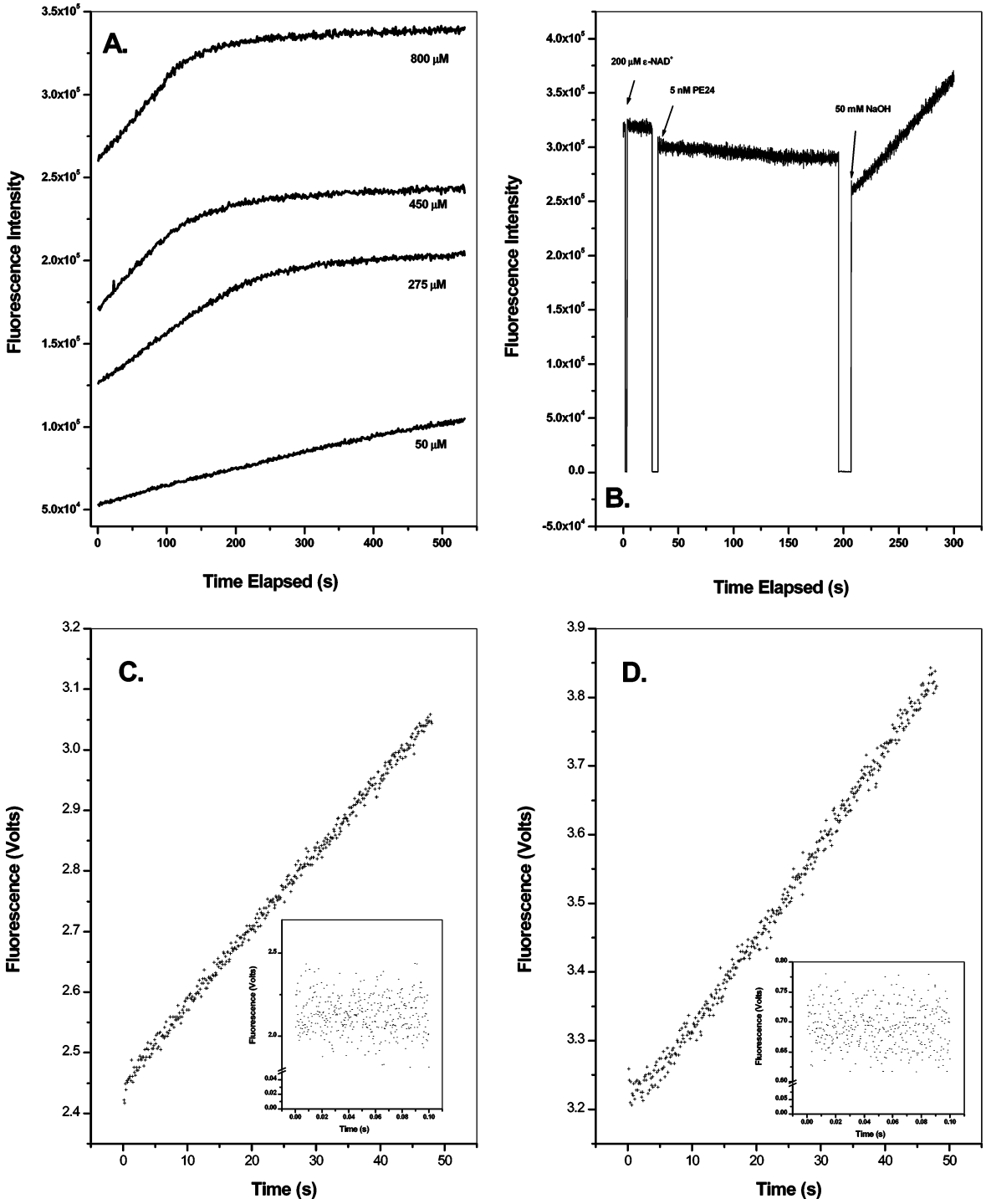

FIGURE 2: Steady-state and pre-steady-state kinetics of PE24H. (A) A set of progress curves for the ADPRT activity of PE24H as a function of ϵ-NAD^+ concentrations. The reactions were conducted as previously described (*17*), and the reaction was linear (50 μM ϵ-NAD^+) for 2 min. The progress curves are shown for 50, 275, 450, and 800 μM ϵ-NAD^+. (B) Kinetic trace for the ADPRT activity of PE24H at 200 μM ϵ-NAD^+ and 5 nM PE24H in 20 mM Tris-HCl, pH 7.9 at 25 °C. The appropriate additions were made as indicated by the arrows to the enzyme-catalyzed reaction being continuously monitored in a fluorescence spectrometer. (C) Kinetic trace showing the fluorescence increase (volts) as a function of time (s) as measured in a stopped-flow spectrometer for base (OH^-)-catalyzed hydrolysis of ϵ-NAD^+ at 25 °C (200 μM NAD^+ and 1 mM NaOH). The inset shows the time course for the reaction from 0 to 100 ms. (D) Stopped-flow kinetic trace for toxin-catalyzed ADPRT reaction at 25 °C and conditions as specified in panel B. The inset also shows the time course for the ADPRT reaction from 0 to 100 ms.

eEF-2, there was no evidence for the formation of a pre-steady-state Michaelis complex between PE24H and ϵ-NAD^+ as monitored by a change in the fluorescence intensity of the etheno moiety (Figure 2D, 0.1−50 s; Figure 2D inset, 1.5−100 ms). In addition, a similar experiment was conducted where the enzyme concentration was increased to approach more closely the ϵ-NAD^+ substrate concentration to facilitate the detection of a pre-steady-state intermediate in the form of a Michaelis complex (PE24H concentration = 0.5 μM), but again, no intermediate was detected (data not shown).

eEF-2 Binding and Rate Constants. The saturable binding of the eEF-2 substrate to the PE24H enzyme is shown in Figure 3A where the binding is measured by the FRET signal

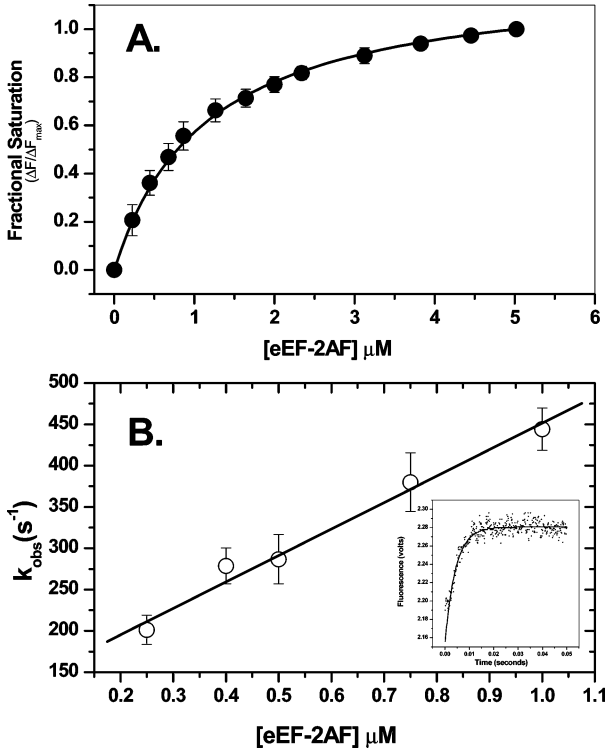

FIGURE 3: eEF-2-AF binding to S585C-AEDANS PE24H. (A) The binding isotherm for eEF-2 with toxin as determined from the quenching of the AEDANS (donor chromophore on PE24H) fluorescence due to FRET to the AF (acceptor) on eEF-2. The raw fluorescence quenching data were converted to fractional saturation values ($\Delta F/\Delta F_{max}$, see Experimental Procedures) and are plotted against the eEF-2-AF concentration. The final concentration of S585C-AEDANS PE24H was 1.0 μM, and NAD^+ was varied between 0 and 6 μM. (B) The dependence of k_{obs} on the concentration of eEF-2-AF (0.25−1.0 μM). The inset shows the time-dependent fluorescence change associated with the binding of 0.8 μM eEF-2-AF to 0.1 μM PE24H.

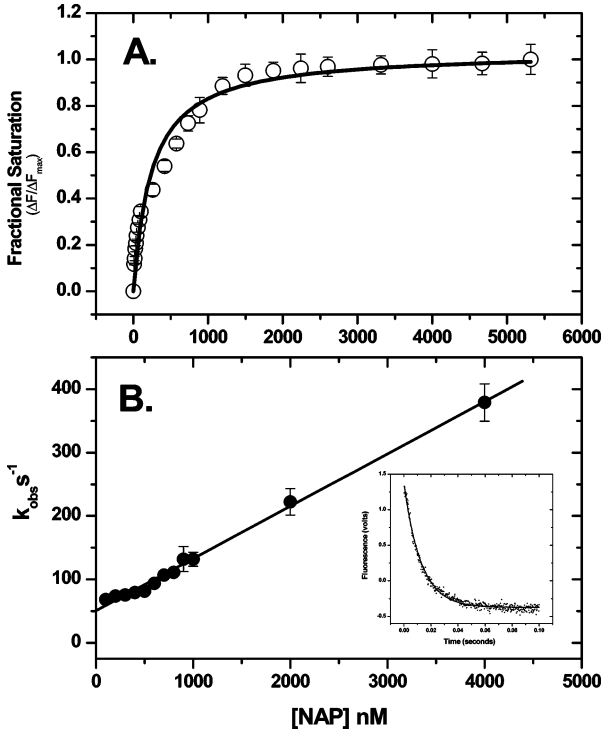

FIGURE 4: NAP binding to PE24H. (A) The binding isotherm for NAP inhibitor with toxin as determined from the quenching of the intrinsic protein fluorescence. The raw fluorescence quenching data were converted to fractional saturation values ($\Delta F/\Delta F_{max}$, see Experimental Procedures) and are plotted against the NAP concentration. The final concentration of PE24H was 1.25 μM, and NAP was varied between 0 and 5.5 μM. (B) The dependence of k_{obs} on the concentration of NAP (0.1−4.0 μM). The inset shows the time-dependent fluorescence change associated with the binding of 1.0 μM NAP to 0.1 μM PE24H.

between the donor (AEDANS) attached to PE24H and the acceptor (fluorescein) attached to eEF-2 as previously characterized (*13*). The dissociation constant for this protein−protein interaction is shown in Table 2 (0.71 ± 0.21 μM) and is in good agreement with our previous report (*13*). The FRET between donor and acceptor results in a 4-fold decrease in AEDANS donor fluorescence upon saturation of the binding of eEF-2 with PE24H (*13*) (data not shown). The apparent (observed) binding rate constant for the eEF-2 substrate with PE24H was measured by stopped-flow fluorescence spectroscopy, the data is shown in Figure 3B, and the plot of fluorescence emission intensity as a function of time at 0.5 μM eEF-2 concentration is shown in the inset. The latter dataset for the time-dependent fluorescence change in eEF-2-AF fluorescence could be fit to a single-exponential function with a rate constant of 286 s^{-1}, and in fact, all of the datasets could be fit with a single-exponential function up to 1.0 μM. Unfortunately, the k_{obs} rate constants were too high to be accurately determined at eEF-2 concentrations above 1 μM. The association and dissociation rate constants, k_{on} and k_{off}, were determined from plots of k_{obs} versus [eEF-2] as explained for NAD^+ binding to the enzyme (see previous section). The values for the association and dissociation rate constants for the protein substrate with the enzyme are also summarized in Table 2. Notably, the dissociation constant (K_d) determined from equilibrium binding experiments was somewhat larger than the value (k_{off}/k_{on}) calculated from the kinetic experiments (Table 2; 0.71 and 0.41 μM, respectively), which generally reflects the difficulty in working with the protein substrate as compared with the dinucleotide, small-molecule substrate, NAD^+. Nonetheless, the two dissociation binding constants are in reasonably good agreement indicating the relative accuracy of the kinetically derived k_{on} and k_{off} rate constants for eEF-2 interaction with PE24H (Table 2). Under pseudo-first-order conditions similar to those used for the determination of k_{cat} for the ADPRT reaction (Table 1; 5 μM eEF-2 at 25 °C), the association rate for the eEF-2 protein with the enzyme is 320 $\mu M^{-1}\ s^{-1} \times 5\ \mu M = 1600\ s^{-1}$, which is approximately 130-fold greater than the k_{cat} value for the ADPRT activity of the toxin (Table 1).

NAP Binding and Rate Constants. The binding curve for the association of the competitive inhibitor (against the NAD^+ substrate), NAP (*5*), is shown in Figure 4A and was measured from the quenching of the intrinsic Trp fluorescence of the enzyme caused by inhibitor docking within the active site near Trps 466 and 558 (*5*−*11*). The inhibitor binding data fit a two-site binding model with a high affinity site (K_d, 0.054 μM) and a lower affinity binding site (K_d, 1.2 μM) (Table 2). However, it was not possible to measure the k_{on} and k_{off} binding rate constants for the high affinity binding site because the binding of NAP at concentrations below 0.1 μM did not cause a sufficiently large decrease in enzyme intrinsic fluorescence to allow accurate detection by stopped-flow spectroscopy. A typical stopped-flow trace for

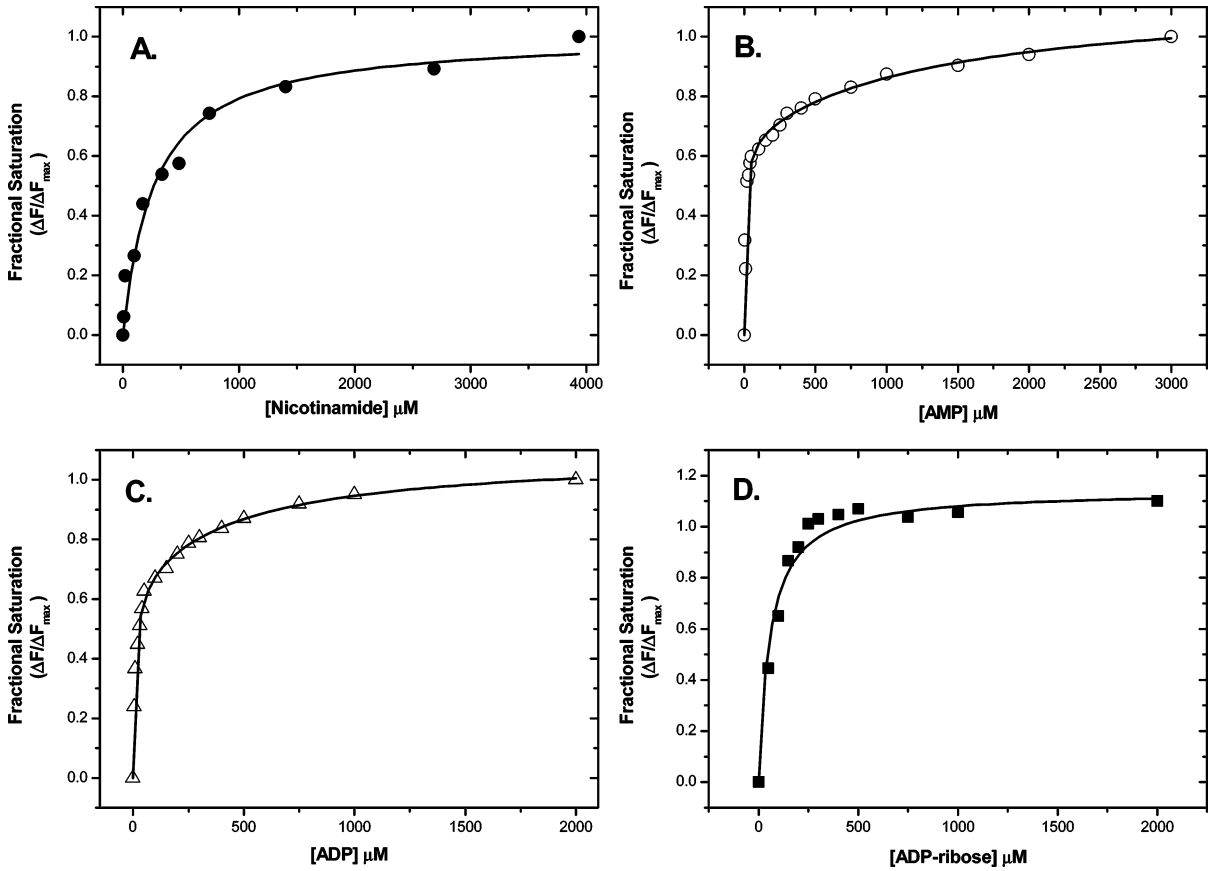

FIGURE 5: Product binding to PE24H. The binding isotherms for (A) nicotinamide, (B) AMP, (C) ADP, and (D) ADP-ribose to PE24H. The raw fluorescence quenching data were converted to fractional saturation values ($\Delta F/\Delta F_{max}$, see Experimental Procedures) and are plotted against the ligand concentration. The final concentration of PE24H was 1.25 μM, and nicotinamide, AMP, ADP, and ADP-ribose were varied between 0 and 4 μM, 0 and 3 μM, 0 and 2 μM, and 0 and 2 μM, respectively. The calculated binding constants are shown in Table 3.

the binding of NAP (0.4 μM) to enzyme is shown in the Figure 4B inset. The k_{obs} calculated from fits of the stopped-flow kinetic traces were plotted against NAP concentration (Figure 4B), and the k_{on} and k_{off} rate constants are shown in Table 2. The K_d value as determined from equilibrium binding experiments (Figure 4A) was nearly 2-fold larger than the value (k_{off}/k_{on}) calculated from the kinetic experiments, which may reflect the difficulty in dissecting the binding rates for the high and lower affinity binding sites because of the inherent lack of sensitivity associated with stopped-flow measurements (caused by reduced signal averaging due to small time constants). Interestingly, it appears that the higher affinity binding of the NAP inhibitor for the NAD^+ subsite within the enzyme is due to a faster k_{on} association rate (82 μM^{-1} s^{-1} as compared with 5 μM^{-1} s^{-1} for NAP and NAD^+, respectively) and a slower k_{off} dissociation rate (51 s^{-1} as compared with 194 s^{-1} for NAP and NAD^+, respectively) than for the NAD^+ substrate (Table 2).

Nicotinamide, AMP, ADP, and ADP-Ribose Binding. One of the products of the ADPRT reaction catalyzed by PE24H is nicotinamide, and the binding isotherm of this product to the enzyme is shown in Figure 5A. Nicotinamide binds with relatively high affinity (K_d = 270 μM, Table 2), but the binding rate constants could not be measured by stopped-flow spectroscopy either because the rates were too fast or because of a lack of sensitivity due to the small change in fluorescence observed when this reaction product/vitamin binds to the active site of the enzyme (data not shown). The second product for the toxin-catalyzed reaction is eEF-2-ADP-ribose, and so the binding of AMP, ADP, and ADP-ribose to toxin was also measured; the binding isotherms are shown in Figure 5B−D,and the equilibrium binding constants are shown in Table 3. Importantly, the binding of the ADP-ribose portion of the NAD^+ substrate does not quench the intrinsic fluorescence of the catalytic domain of the toxin to nearly the extent that nicotinamide binding does. Furthermore, the combined fluorescence quenching caused by the two components of the NAD^+ substrate, nicotinamide and ADP-ribose, does not account for the magnitude of the fluorescence quenching caused by the intact NAD^+ substrate [83% and (32 + 16 = 48%) for NAD^+ and nicotinamide + ADP-ribose, respectively; Table 3]. This observation indicates that when NAD^+ binds to the enzyme, it must invoke

Table 3: Binding Constants and Fluorescence Quenching by NAD^+ Substrate and the Products of the ADPRT Reaction

parameter	NAD^+	nicotinamide	AMP	ADP	ADP-ribose
$K_{d\,(1)}$[a] (μM)	47 ± 5	270 ± 49	9 ± 2	9 ± 1	58 ± 11
$K_{d\,(2)}$[b] (μM)			1330 ± 350	438 ± 97	
% FQ[c]	83 ± 12	32 ± 6	29 ± 4	15 ± 2	16 ± 2

[a] Determined from the nonlinear fit of fluorescence quenching data to a single-site binding model as described in Experimental Procedures. [b] Determined from the nonlinear fit of fluorescence quenching data to a two-site binding model as described in Experimental Procedures. [c] Percent fluorescence quenching (% FQ) as determined from the extent of quenching of the intrinsic PE24H protein fluorescence at saturating concentration of ligand (note: % residual fluorescence = 100 − %FQ).

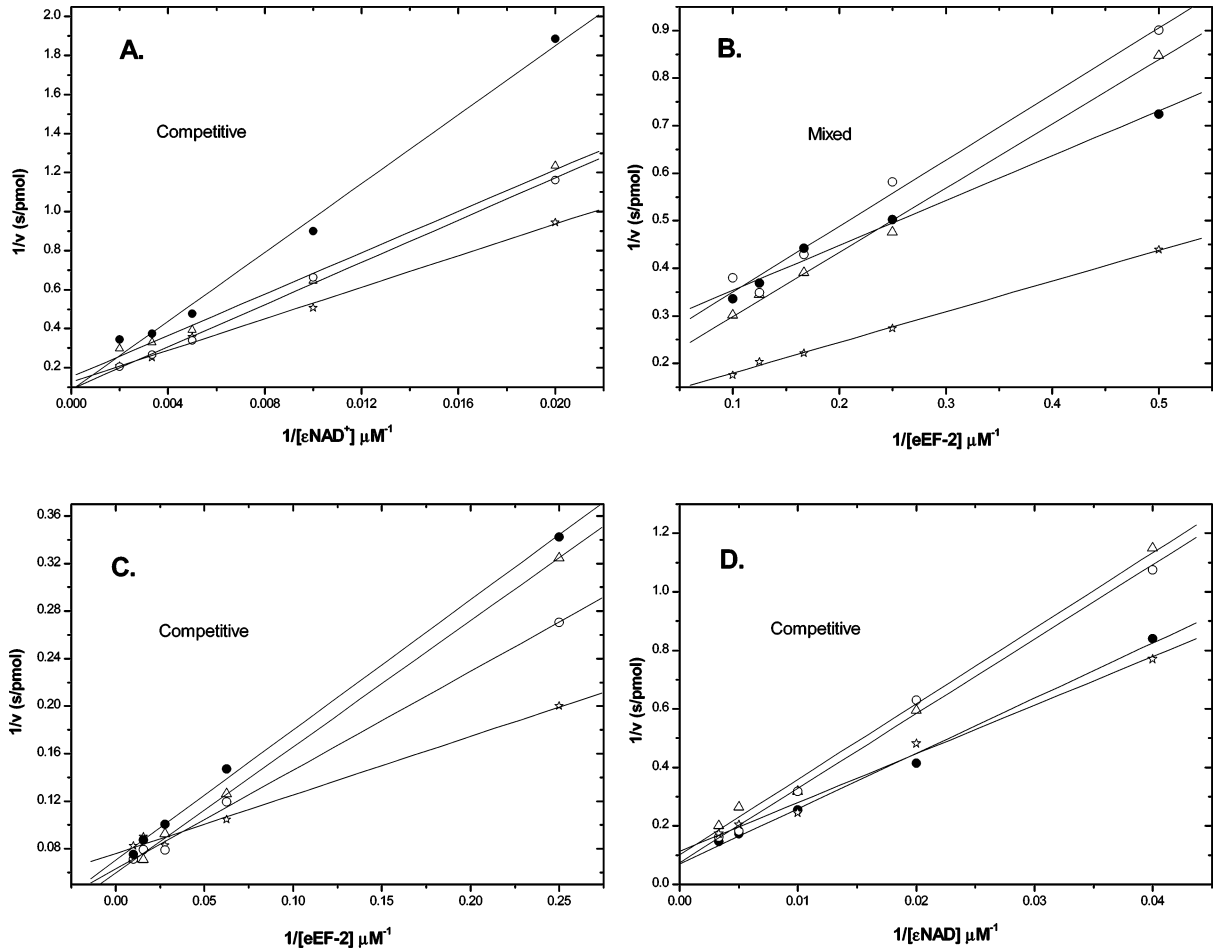

FIGURE 6: Product inhibition plots of ADPRT activity of PE24H. Product inhibition studies were conducted with (A) nicotinamide with variable ϵNAD$^+$ substrate, (B) nicotinamide with variable eEF-2 substrate, (C) eEF-2-ADPr with variable ϵNAD$^+$ substrate, and (D) eEF-2-ADPr with variable eEF-2 substrate. Nicotinamide was introduced as the product inhibitor in panels A and B at 0, 25, 50, and 100 μM. eEF-2-ADPr was used as the inhibitor in panels C and D at 0, 5, 6, and 7 μM.

a specific structural change within the active site of the enzyme that is largely responsible for the 6-fold decrease of the intrinsic Trp fluorescence (ref *12*; Table 3).

Product Inhibition Studies. The mechanism for the toxin-catalyzed ADPRT reaction has proved elusive and has been a source of controversy (*11*−*13*, *33*, *34*). More recently, however, studies have intimated that the ADPRT reaction may be a random order ternary-complex type mechanism (*12*, *13*, *36*). However, to provide more conclusive evidence for the specific reaction mechanism, we used inhibitors that would be expected to compete with one of the substrates for a site on the enzyme. The two major products for the reaction catalyzed by PE24H are nicotinamide and eEF-2-ADP-ribose (a H$^+$ is also a product of the reaction but was not considered since its concentration is controlled by the buffer in the reaction solution). Nicotinamide, when present as an inhibitor for the ADPRT reaction, showed competitive inhibition when the ϵNAD$^+$ substrate was varied (Figure 6A) and mixed-type inhibition when the eEF-2 was the variable substrate (Figure 6B). Furthermore, when eEF-2-ADP-ribose was the inhibitor, competitive inhibition was observed for both conditions where eEF-2 or ϵNAD$^+$ were the variable substrates (Figure 6C,D). According to the Cleland rules, this indicates that the ADPRT reaction catalyzed by the *Pseudomonas* toxin is, indeed, a random-order ternary complex mechanism (see Discussion).

Sigmoidal Kinetics of eEF-2 Substrate. The eEF-2 substrate shows sigmoidal kinetic behavior with the PE24H enzyme (Figure 7A), which is usually indicative of a multimeric enzyme that is capable of cooperative behavior (*37*). In contrast, the NAD$^+$ substrate shows conventional Michaelis−Menten kinetic behavior with the toxin-enzyme (*17*). Intriguingly, PE24H is a single subunit enzyme (*9*, *10*) and possesses a single active site per molecule (*5*−*12*, *34*) and hence should not be capable of sigmoidal kinetic behavior. The kinetic data shown in Figure 7A were plotted according to the Eadie−Hofstee linear transformation of the Michaelis−Menten equation: $v_o = V_{max}[S]^n/K_m + [S]^n$ for $n = 1$ (Figure 7B inset) and $n = 2$ (Figure 7B). It is clear that the data do not fit the standard Michaelis−Menten equation and model but rather fit the model for two substrate-binding sites with positive cooperativity (*31*). To investigate the possibility that the eEF-2 protein substrate was the source of the cooperative kinetic behavior, a sample of purified wheat germ eEF-2 was divided into two parts; one part was labeled with IAEDANS (*19*), and the other was labeled with 5-IAF (*13*) to ascertain the oligomeric state of eEF-2 by FRET analysis. Fluorescence emission spectra were collected for the eEF-2-AEDANS protein in solution in the absence and presence of the eEF-2-AF protein (Figure 7C). It is clear from the data in Figure 7C that FRET is occurring between the AEDANS (donor) moiety and the AF (acceptor) moiety

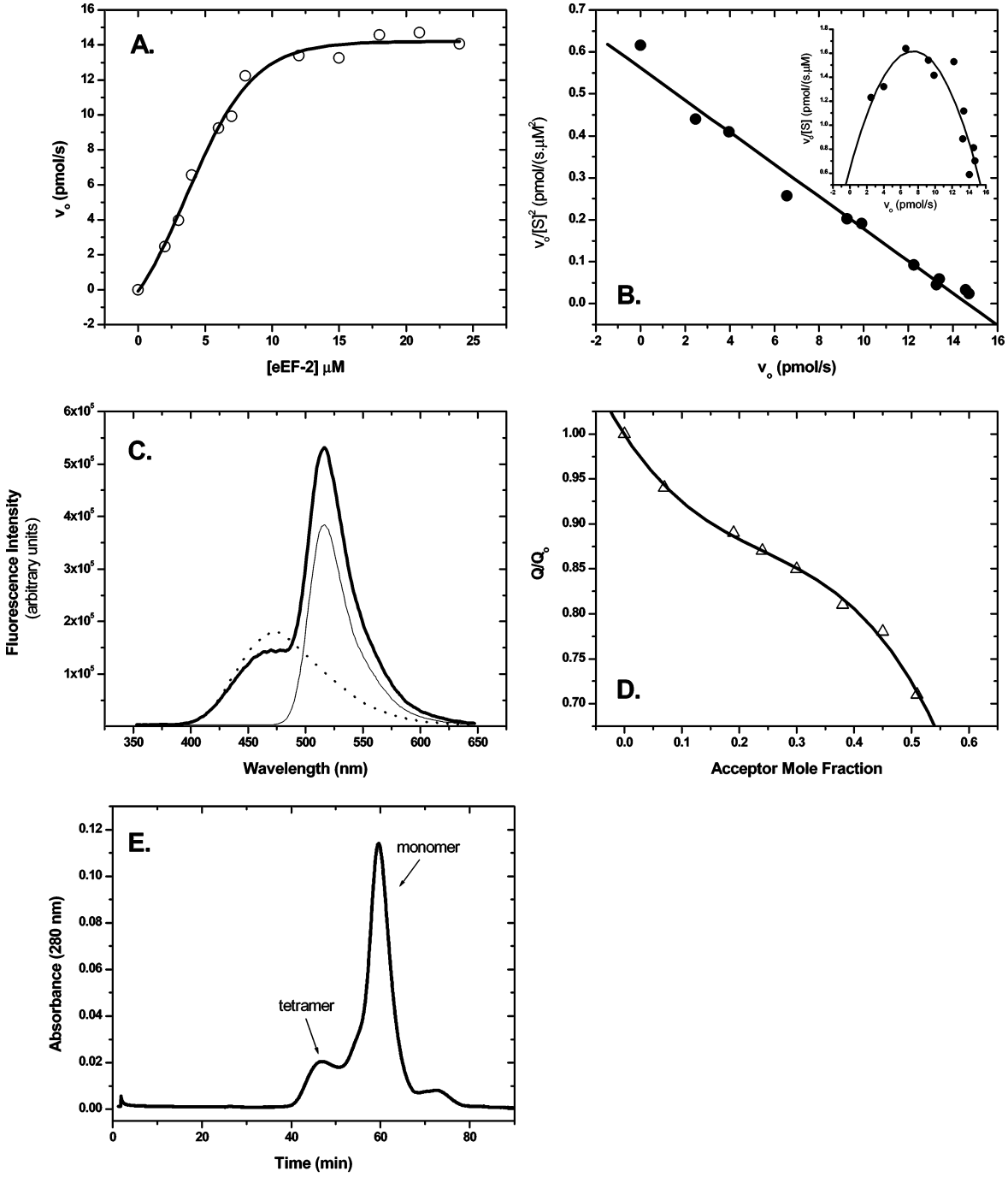

FIGURE 7: Oligomeric behavior of eEF-2. (A) Sigmoidal kinetics of eEF-2 as substrate for ADPRT activity of PE24H. The ADPRT activity of PE24H was measured as described in Experimental Procedures and in ref *17*. (B) Eadie−Hofstee plot of kinetic data from a (A) fit according to the standard Michaelis−Menten equation (inset) and according to the modified equation (where $n = 2$ for $[S]^n$) $\upsilon_0 = V_{max}[S]^2/(K_m + [S]^2)$ (large graph). (C) Evidence for FRET between eEF-2-AEDANS and eEF-2-AF. Fluorescence emission spectra of 6 μM eEF-2-AEDANS in buffer (dotted line), 6 μM eEF-2-AF in buffer (thin line), 6 μM eEF-2-AEDANS, and 6 μM eEF-2-AF in buffer. Measurements were conducted in 20 mM Tris-HCl, 50 mM KCl, pH 7.9 buffer at 25 °C. (D) Relative fluorescence quantum yield of eEF-2-AEDANS, the energy donor, as a function of the mole fraction of eEF-2-AF (acceptor). The data were fit to a third-order polynomial (tetramer model) as described in Experimental Procedures and described by Veatch and Stryer (*28*). (E) Analytical gel filtration of wheat germ eEF-2. A 200 μL sample of purified wheat germ eEF-2 in 20 mM Tris-HCl, 100 mM NaCl, pH 7.9 buffer was injected onto a Superose-6 column (1.2 cm diameter × 30 cm length, equilibrated in the same buffer) with a flow rate of 0.5 mL/min (see Experimental Procedures for details).

from adjacent eEF-2 protein molecules as witnessed by the decrease in AEDANS donor fluorescence concomitant with an increase in AF acceptor fluorescence (Figure 7C, bold line). The R_o values for this donor−acceptor pair range from 46 to 56 Å (*38*), and given the dimensions of this protein (75 × 130 Å; ref *39*) and the dilute solution concentrations used in the FRET experiment (Figure 7B), intermolecular association is an obvious conclusion. The eEF-2-AEDANS protein was titrated with the eEF-2-AF protein, and the AEDANS donor fluorescence was plotted against the mole fraction of the AF acceptor species (Figure 7D). The data in Figure 7C,D suggest that wheat germ eEF-2 is oligomeric in solution, and the data were fit to a third-order polynomial (*28*), which implies a tetrameric state for this ribosome

Scheme 1

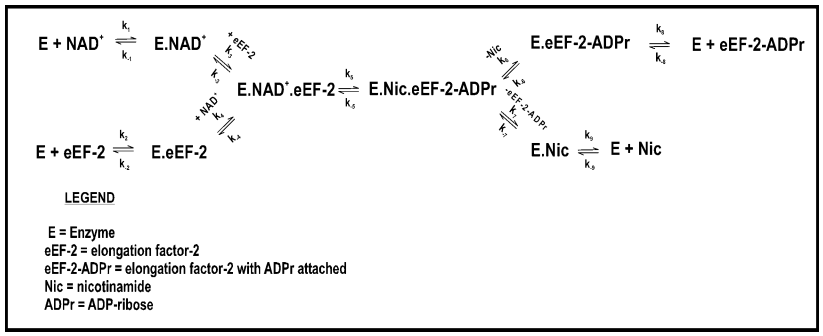

translocase in solution. This result was substantiated by analytical gel filtration experiments where wheat germ eEF-2 was shown to exist in solution as an equilibrium between monomeric and tetrameric species (Figure 7E).

DISCUSSION

Pre-Steady-State Kinetics. The data shown in Figure 2 indicate that there is no pre-steady-state intermediate that forms during either the OH^--catalyzed hydrolysis of NAD^+ or the diphthamide-catalyzed scission of the C−N bond between the nicotinamide N1 and C1 of the adjacent ribose moiety. This indicates that the rate measured in the standard fluorescence-based kinetic ADPRT assay reflects a rather slow event occurring during the transferase reaction catalyzed by the enzyme. It appears from detailed steady-state kinetic analysis as well as stopped-flow kinetic measurements that the fluorescence increase observed during the steady state reaction is likely due to the breaking of the glycosidic bond within ϵ-NAD^+ and is not a result of a separation of the two bases within NAD^+ associated with substrate binding to the enzyme active site (*31*). Furthermore, there is no evidence for a covalent enzyme intermediate in the catalytic cycle nor is the release of the products, nicotinamide and eEF-2-ADPr, rate-limiting for the reaction (Figure 2; data not shown). These conclusions agree with the studies conducted by Berti et al. (*18*), who showed that the transition state structure of the hydrolysis reaction of NAD^+ catalyzed by DT involves an oxocarbenium ion with low residual bond order to the leaving group and low bond order to the approaching nucleophile, water. It was determined that the reaction mechanism is concerted and highly asynchronous with both the leaving group and the nucleophile participating in the reaction coordinate. However, there are significant differences between the nonphysiologically relevant hydrolysis reaction and the diphthamide-specific transferase reaction catalyzed by DT and ETA in both reaction mechanism details and rates (*18*, *19*). A high-resolution structure of the complex between these enzymes and their protein substrate, eEF-2, is needed to facilitate further kinetic analyses in the quest to understand the details of the ADP-ribosyltransferase reaction.

Substrate Binding and Rate Constants. The data shown in Figures 1 and 3 represent the first report of the kinetics for the binding of the NAD^+ as well as the eEF-2 substrate for ETA. Under pseudo-first-order conditions where both substrates are at saturating concentrations, the NAD^+ substrate binds to the enzyme with a slightly faster association rate constant (k_{on}) than the eEF-2 substrate ($4.7\ \mu M^{-1}\ s^{-1} \times 500\ \mu M = 2350\ s^{-1}$ and $320\ \mu M^{-1}\ s^{-1} \times 5\ \mu M = 1600\ s^{-1}$, respectively; Table 2). Importantly, the accuracy of the rate constant measurements is high since the dissociation constants (K_d) compare favorably in value as determined from equilibrium binding experiments and the ratio of the dissociation and association rate constants (Table 2). Overall, these kinetic data indicate that the eEF-2 binding step is not the rate-determining step for the reaction, that the rate-limiting step must involve some aspect of the ADP-ribose transfer portion of the reaction to the nucleophilic diphthamide residue within the eEF-2 substrate, and that this event may occur deep within the heart of the enzyme during catalysis.

Structural Changes within PE24H Invoked by NAD^+ Binding. Previous work in our laboratory indicated that NAD^+ induces a significant structural change within the catalytic domain of ETA upon binding to the enzyme (*12*). This was further substantiated upon the comparison of the binding of various parts of the NAD^+ molecule to the PE24H enzyme with the binding of intact NAD^+ substrate as monitored by changes in the intrinsic fluorescence of the enzyme (Table 3). These data also suggest that upon scission of the glycosidic bond within NAD^+ that there is a significant structural change (relaxation) that occurs within the catalytic domain that may be associated with product release (*33*). It must be noted that product release is very fast and could not be detected within the dead-time of the stopped flow instrument used in these experiments ($t_d = 1.5$ ms). These data indicate that the toxin-enzyme is using its structural flexibility as a catalytic aid to facilitate the ribosyltransferase reaction.

Product Inhibition Studies. The use of reaction products that may function as inhibitors that compete with one of the substrates for a site on an enzyme can give useful information as to the mechanism of that reaction (*40*). A product of the reaction, if present in the initial catalytic mixture, may be expected to compete with one of the substrates for a binding site on an enzyme, and this would be observed as a decrease in the rate of the forward reaction. Cleland has formulated a set of rules that enable the inhibition patterns for a particular mechanism to be predicted (*41*). The pattern of inhibition that was observed for the toxin-catalyzed ADPRT reaction was competitive for nicotinamide inhibition with a variable ϵNAD^+ substrate and also for eEF-2-ADPr inhibition with a variable eEF-2 substrate. The pattern was mixed and competitive for the nicotinamide inhibition with a variable eEF-2 substrate and for eEF-2-ADPr inhibition with a variable ϵNAD^+ substrate, respectively. This inhibition pattern is indicative of a random-order ternary complex mechanism for the PE24H enzyme (see Scheme 1), which

confirms recent proposals for the ADPRT reaction (*11*−*13*, *23*, *35*).

In this study, we have determined the following rate constants and values (refer to Scheme 1): k_1 (4.1 s^{-1}), k_{-1} (194 s^{-1}), k_2 (320 s^{-1}), and k_{-2} (131 s^{-1}). We were unable to determine the rate constants for nicotinamide (k_9 and k_{-9}) and eEF-2-ADPr (k_8 and k_{-8}) interaction with enzyme due to the rapid nature of these events. We have not yet been able to design suitable experiments to measure the rates of eEF-2 binding to the E-NAD^+ complex (k_3 and k_{-3}) and NAD^+ binding to the E-eEF-2 complex (k_4 and k_{-4}) due to interference of the fluorescence signal being monitored. Furthermore, the rate constants, k_5 and k_{-5}, represent the intrinsic rate for the nucleophilic substitution reaction, which may be the rate-limiting step for the enzyme (Figure 2A−D); however, it cannot be proven without first measuring all of the rate constants for each of the reaction steps. We have also not yet attempted to measure the product release rates from the ternary complex for either nicotinamide (k_6 and k_{-6}) or for eEF-2-ADPr (k_7 and k_{-7}). Clearly, further kinetic studies await completion before the detailed mechanism for the ADPRT activity of ETA can be known.

Sigmoidal Kinetics of the eEF-2 Substrate. Initially, the sigmoidal behavior observed for the toxin-enzyme when the eEF-2 protein substrate was varied in the ADPRT reaction was surprising since the catalytic domain of the toxin, PE24H, is a single subunit, monomeric enzyme with a single substrate-binding site for NAD^+ (*9*−*10*). However, there are previous examples where alternative kinetic explanations were invoked to describe the sigmoidal responses of simple enzyme systems (*37*). Jensen and Trentini (*42*) interpreted the kinetics of 3-deoxy-D-arabino-heptulosonate-7-phosphate synthetase of *Rhodomicrobium vannielii* in terms of a preferred (but not exclusive) kinetic pathway to a ternary complex. Furthermore, Segel gives an excellent treatise on this subject (*37*). The possibility exists that for the toxin-catalyzed ADPRT reaction the preferred pathway is for the eEF-2 protein substrate to initially bind followed by the NAD^+ substrate. If the reverse order of substrate binding occurs, which might be expected at high NAD^+ concentration and low eEF-2 concentration, then the reaction still occurs but is not as kinetically favorable as the former mechanism. This mechanism could account for the sigmoidal shape of the Michaelis plot for the eEF-2 substrate (Figure 7A). However, the finding that eEF-2 is oligomeric in solution (Figure 7D) presents another possible explanation for the sigmoidal kinetic behavior for this substrate. Initial experiments indicated that the FRET efficiency occurring within eEF-2 oligomers is markedly reduced upon dilution of the protein to a concentration below 2 μM in solution. This suggests the possibility of a monomer−oligomer equilibrium that may have a K_d that corresponds with the sigmoidal shift in the Michaelis plot for ADPRT activity (Figure 7A). These data suggest that the aggregation state of eEF-2 may be that of a tetramer in solution (Figure 7D). Furthermore, analytical gel filtration experiments showed that the predominant oligomeric form of wheat germ eEF-2 in solution is a tetramer (Figure 7E). Exactly what, if any, the ramifications of the oligomeric nature of the ribosome translocase may have on its in vivo function within the eukaryotic cell and at the ribosome must await further characterization. Furthermore, experiments are being conducted to more fully characterize the individual kinetic steps for the ADPRT reaction catalyzed by the toxin-enzyme.

ACKNOWLEDGMENT

We thank Gerry Prentice and Dave Teal for expert technical support and assistance during the tenure of this work.

REFERENCES

1. Vasil, M. L., and Ochsner, U. A. (1999) *Mol. Microbiol. 34*, 399−413.
2. Stanislavsky, E. S. (1980) *Zh. Microbiol. Epidemiol. Immunobiol. 12*, 91−96.
3. Emori, T. G., and Gaynes, R. P. (1993) *Clin. Microbiol. Rev. 6*, 428−442.
4. Diekema, D. J., Pfaller, M. A., Jones, R. N., Doern, G. V., Winokur, P. L., Gales, A. C., Sader, H. S., Kugler, K., and Beach, M. (1999) *Clin. Infect. Dis. 29*, 595−607.
5. Armstrong, S., Li, J. H., Zhang, J., and Merrill, A. R. (2002) *J. Enzyme Inhib. Med. Chem. 17*, 235−246.
6. Barth, H., Preiss, J. C., Hofmann, F., and. Aktories, K. (1999) *J. Biol. Chem. 273*, 29506−29511.
7. Wick, M. J., Hamood, A. N., and Iglewski, B. H. (1990) *Mol. Microbiol. 4*, 527−535.
8. Caputo, G. A., and London, E. (2003) *Biochemistry 42*, 3275−3285.
9. Li, M., Dyda, F., Benhar, I., Pastan, I., and Davies, D. R. (1996) *Proc. Natl. Acad. Sci. U.S.A 93*, 6902−6906.
10. Li, M., Dyda, F., Benhar, I., Pastan, I., and Davies, D. R. (1995) *Proc. Natl. Acad. Sci. U.S.A 92*, 9308−9312.
11. Beattie, B. K., Prentice, G. A., and Merrill, A. R. (1996) *Biochemistry 35*, 15134−15142.
12. Beattie, B. K., and Merrill, A. R. (1999) *J. Biol. Chem. 274*, 15646−15654.
13. Armstrong, S., Yates, S. P., and Merrill, A. R. (2002) *J. Biol. Chem. 277*, 46669−46675.
14. Carroll, S. F., and Collier, R. J. (1988) *Methods Enzymol. 165*, 218−225.
15. Wilson, B. A., Reich, K. A., Weinstein, B. R., and Collier, R. J. (1990) *Biochemistry 29*, 8643−8651.
16. Wilson, B. A., and Collier, R. J. (1992) *Curr. Top. Microbiol. Immunol. 175*, 27−41.
17. Wilson, B. A., Blanke, S. R., Reich, K. A., and Collier, R. J. (1994) *J. Biol. Chem. 269*, 23296−23301.
18. Berti, P. J., Blanke, S. R., and Schramm, V. L. (1997) *J. Am. Chem. Soc. 119*, 12079−12088.
19. Berti, P. J., and Schramm, V. L. (1997) *J. Am. Chem. Soc. 119*, 12069−12078.
20. Wilson, B. A., and Collier, R. J. (1992) *Curr. Top. Microbiol. Immunol. 175*, 27−41.
21. Carroll, S. F., McCloskey, J. A., Crain, P. F., Oppenheimer, N. J., Marschner, T. M., and Collier, R. J. (1985) *Proc. Natl. Acad. Sci. U.S.A. 82*, 7237−7241.
22. Carroll, S. F., and Collier, R. J. (1984) *Proc. Natl. Acad. Sci. U.S.A. 81*, 3307−3311.
23. Armstrong, S., and Merrill, A. R. (2001) *Anal. Biochem. 292*, 26−33.
24. Yates, S. P., and Merrill, A. R. (2001) *J. Biol. Chem. 276*, 35029−35036.
25. Andrews, P. (1970) in *Methods of Biochemical Analysis* (Glick, D., Ed.) pp 1−49, Interscience, New York.
26. Beattie, B. K., and Merrill, A. R. (1996) *Biochemistry 35*, 9042−9051.
27. Mohammadi, F., Prentice, G. A., and Merrill, A. R. (2001) *Biochemistry 40*, 10273−10283.
28. Veatch, W., and Stryer, L. (1977) *J. Mol. Biol. 113*, 89−102.
29. Tory, M. C., and Merrill, A. R. (1999) *J. Biol. Chem. 274*, 24539−24549.
30. Mutai, K., Gruber, B. A., and Leonard, N. J. (1975) *J. Am. Chem. Soc. 97*, 4095−4104.
31. Barrio, J. R., Secrist, J. A., III, and Leonard, N. J. (1972) *Proc. Natl. Acad. Sci. U.S.A. 69*, 2039−2042.

32. Leonard, N. J. (1984) *CRC Crit. Rev. Biochem. 15*, 125−199.
33. Bell, C. E., Yeates, T. O., and Eisenberg, D. (1997) *Protein Sci. 6*, 2084−2096.
34. Saelinger, C. B. (1988) *Methods Enzymol. 165*, 226−231.
35. El Zaim, H. S., Chopra, A. K., Peterson, J. W., Vasil, M. L., and Heggers, J. P. (1998) *Infect. Immun. 66*, 5551−5554.
36. Beattie, B. K., and Merrill, A. R. (1996) *Biochemistry 35*, 9042−9051.
37. Segal, I. H. (1975) *Enzyme Kinetics: Behaviour and Analysis of Rapid Equilibrium and Steady-State Enzyme Systems*, 1st ed., pp 369−384, John Wiley & Sons, Inc., New York.
38. Wu, P., and Brand, L. (1994) *Anal. Biochem. 218*, 1−13.
39. Jørgensen, R., Ortiz, P. A., Carr-Schmid, A., Nissen, P., Kinzy, T. G., and Andersen, R. G. (2003) *Nat. Struct. Biol. 10*, 379−385.
40. Cleland, W. W. (1970) *Steady-state kinetics*, 3rd ed.[2], pp 1−65, Academic Press, New York.
41. Cleland, W. W. (1967) *Enzyme Kinetics*, pp 36, 77−120, Academic Press, New York.
42. Jensen, R. A., and Trentini, W. C. (1970) *J. Biol. Chem. 245*, 2018−2022.

BI034772U